Scientific Reports

https://doi.org/10.1038/s41598-026-40291-2

Article in Press

Lectin-based detection and expression profiling of native glycoRNAs

Received: 28 May 2025

Accepted: 11 February 2026

Published online: 14 February 2026

Cite this article as: Li Y., Qian Y., Li X. *et al.* Lectin-based detection and expression profiling of native glycoRNAs. *Sci Rep* (2026). https://doi.org/10.1038/s41598-026-40291-2

Yong Li, Yisong Qian, Xiang Li, Tianhua Lei, Hillary McGraw, Paula Monaghan-Nichols & Mingui Fu

Lectin-based detection and expression profiling of native glycoRNAs

Yong Li[1, 2], Yisong Qian[3], Xiang Li[1], Tianhua Lei[1], Hillary McGraw[4], Paula Monaghan-Nichols[1], Mingui Fu[1‡]

[1]Department of Biomedical Science, School of Medicine, University of Missouri Kansas City, Kansas City, MO 64108, United States
[2]Department of Anesthesia, The first affiliated hospital, Nanchang University, Nanchang, Jiangxi 330006, China
[3]Key Lab for Arteriosclerology of Hunan Province, International Joint Laboratory for Arteriosclerotic Disease Research of Hunan Province, Institute of Cardiovascular Disease, University of South China, Hengyang 421001, China
[4]Division of Biological and Biomedical Systems, School of Science and Engineering, University of Missouri Kansas City, Kansas City, MO 64110, United States

[‡]Corresponding author: Mingui Fu, fum@umkc.edu

Abstract

Current methods for detecting glycoRNAs include metabolic labeling in living cells or animals and RNA-optimized periodate oxidation and aldehyde labeling (rPAL), each of which offers distinct advantages and limitations. Here, we report a relatively simple and rapid approach for detecting native glycoRNAs using direct lectin hybridization. This method involves several straightforward steps, including total RNA isolation, northern blotting, and lectin hybridization. Its advantages include high sensitivity, procedural simplicity, and broad applicability. Using this approach, we profiled glycoRNA expressions in RNA samples derived from human and murine tissues and cell lines and compared the results with those obtained using two established detection methods. We also examined differences in glycoRNA expression under physiological and pathological conditions. Notably, we report for the first time the detection of free glycoRNAs in various human biofluids, including plasma, urine, and amniotic fluid. Overall, our findings demonstrate that this method is reliable and reproducible, providing an alternative tool for studying glycoRNA biology and potentially offering utility for future clinical diagnostics.

Keywords: glycoRNAs, rPAL, lectin, expression profiling, detection

Introduction

RNAs have traditionally been viewed as localizing and functioning within the cytoplasm and nucleus of mammalian cells. However, recent advances have uncovered a surprising aspect of RNA biology: the presence of specific RNA molecules on the outer surface of mammalian cells (1–3). Among the most intriguing discoveries is the identification of glycoRNAs—small noncoding RNAs covalently modified with complex N-glycans—that are synthesized intracellularly but localized to the cell surface (2). Although their precise functions remain unclear, accumulating evidence suggests that glycoRNAs play pivotal roles in immune responses, host–pathogen interactions, and cancer growth and metastasis (4–10).

Zhang et al. reported that cell-surface glycoRNAs mediate neutrophil recruitment to inflammatory sites through selective interactions with adhesion molecules on vascular endothelial cells, such as P-selectin (4). We recently identified two forms of glycoRNAs, termed glycoRNA-L and glycoRNA-S, which are robustly expressed in human monocytes and facilitate interactions between monocytes and endothelial cells via binding to Siglec-

5 (5). In addition, two recent studies demonstrated that modified small nuclear RNAs (snRNAs) and their associated proteins, such as histones, when present on the cell surface, can trigger inflammatory responses (6, 7). Moreover, Xie et al. identified acpU3 as the glycan attachment site on RNA molecules (11). Perr et al. further revealed that glycoRNAs form microdomains with RNA-binding proteins on the cell-surface membrane, which may serve as entry points for permeable peptides, viruses, or nutrients (12). Collectively, these discoveries open a new avenue for investigating the molecular mechanisms underlying immune regulation, cell–cell communication, host–pathogen interactions, embryogenesis, and cancer metastasis.

Current methods for detecting glycoRNAs include metabolic labeling of living cells or animals (2, 13) and RNA-optimized periodate oxidation and aldehyde ligation (rPAL), which directly detects native glycoRNAs through periodate oxidation and aldehyde ligation (11). Each method has distinct advantages and limitations. For example, metabolic labeling relies on living cells or organisms that must uptake labeling molecules prior to biosynthetic processing and incorporation into nascent biopolymers such as glycans. Consequently, this approach is restricted to experimental contexts in which labeled cells or organisms are accessible. rPAL, in contrast, offers high sensitivity and enables detection of native RNA samples; however, it selectively detects sialoglycoRNAs and does not capture other glycoforms.

In this study, we developed a relatively simple and rapid method for detecting native glycoRNAs using direct lectin hybridization, termed lectin-based detection (LBD). We compared LBD with the two established approaches, metabolic labeling and rPAL, and applied it to profile glycoRNA expression across a variety of human and murine tissues and cell lines. Overall, this lectin-based method provides a practical alternative for studying glycoRNA biology and may have potential utility in future clinical diagnostics.

Results

Screening lectins for the detection of native glycoRNAs

To identify lectins suitable for detecting native glycoRNAs, we screened 24 commercially available lectins purchased from Vector Laboratories. Total RNA isolated from THP-1 cells, a human monocyte cell line, was used for this analysis. Most of the lectins tested were capable of detecting glycoRNAs (**Fig. 1a**), revealing a band of the same apparent size as that detected by rPAL. This suggests that lectin-based detection identifies the same glycoRNA species as rPAL.

Among the 24 lectins tested, *Lycopersicon esculentum* lectin (LEL), *Datura stramonium* lectin (DSL), *Solanum tuberosum* lectin (STL), and wheat germ agglutinin (WGA) produced the strongest signals. Notably, these lectins preferentially bind N-acetylglucosamine (**Fig. 1b**). Other lectins, including MAL-II, SNA, Con A, SBA, RCA I, PHA-E, UEA-1, DBA, PNA, Jacalin, VVL, LCA, PSA, and ECL, also detected the same band but with weaker signals. Because these lectins recognize mannose, fucose, sialic acid, galactose, and N-acetylgalactosamine, these results suggest that glycoRNAs in THP-1 cells possess complex glycan structures containing these monosaccharides, with a relative enrichment in N-acetylglucosamine.

Siglec-5, a recombinant human lectin, also detected glycoRNAs with a strong signal; however, the band appeared sharper and more condensed. In contrast, although WGA produced a strong signal, succinylated WGA (S-WGA) failed to detect the glycoRNA band. We further tested these lectins using RNA samples from HeLa and HEK293 cells. While the overall detection patterns were similar, the apparent band sizes differed among the three cell lines (data not shown), suggesting the presence of cell type–specific glycoRNA species.

Collectively, these results demonstrate that lectins can be directly used to detect glycoRNAs in native RNA samples and may be useful for distinguishing distinct glycoRNA populations across different cell types. Because LEL produced the strongest signal, it was selected as the probe for subsequent optimization of the detection protocol.

Optimizing conditions for lectin-based detection of glycoRNAs

Next, we optimized the experimental conditions for lectin-based detection of glycoRNAs. Total RNA isolated from THP-1 cells was used for all optimization experiments. Biotinylated *Lycopersicon esculentum* lectin (LEL, 3 μg/ml) served as the probe for hybridization. We first evaluated RNA transfer conditions using three different transfer buffers: a commercial buffer from Invitrogen, 2× SSC, and 3 M NaCl (pH 1.0). Although RNA transfer efficiency was highest with 3 M NaCl, as previously reported by Xie et al. (11), the Invitrogen transfer buffer produced a cleaner background. The 2× SSC buffer also yielded a low background and offered a more cost-effective alternative (**Fig. S1a**).

Next, we compared two membrane types: nitrocellulose and nylon. Although nylon membranes are commonly used for northern blotting, they generated a high background signal in this assay and were therefore unsuitable for lectin-based detection (**Fig. S1b**). In contrast, nitrocellulose membranes produced cleaner results. We then optimized blocking conditions. A protein-free blocking buffer from LI-COR Biosciences resulted in the lowest background compared with 0.5% bovine serum albumin (BSA) or 5% milk. Although 0.5% BSA was acceptable, skim milk was unsuitable due to strong background signals, likely caused by the presence of carbohydrates (**Fig. S1c**).

Finally, we optimized the concentration of LEL and the incubation time. An LEL concentration of 3 μg/ml yielded strong and reproducible signals (**Fig. S1d**). While a 24-hour incubation produced the strongest signal, shorter incubation times of 2–4 hours still generated robust and usable signals (**Fig. S1e**).

Sensitivity and specificity of lectin-based detection of native glycoRNAs

Next, we compared the sensitivity of lectin-based detection using LEL with that of metabolic labeling and rPAL. As shown in **Fig. 2a**, LEL exhibited sensitivity comparable to both metabolic labeling and rPAL, with a minimum detectable input of approximately 0.5 μg of total RNA. As we previously reported (5), two glycoRNA species—designated glycoRNA-L and glycoRNA-S—can be detected in THP-1 cells by metabolic labeling with Ac_4ManNAz. However, the smaller glycoRNA species (glycoRNA-S) were not detected by either LEL or rPAL. GlycoRNA-S was selectively labeled by N-acetylgalactosamine–azide in both THP-1 and HeLa cells (5), suggesting that it may possess a relatively simple glycan structure composed of approximately 3–5 N-acetylgalactosamine residues (14). Consequently, rPAL, which detects sialylated glycans, and LEL, which preferentially binds N-acetylglucosamine, may fail to detect this glycoRNA species. Notably, Sharma et al. also reported the existence of two distinct populations of glycoRNAs in secreted exosomes (15). Nevertheless, the precise identities and structures of glycoRNA-L and glycoRNA-S require further investigation.

To assess the specificity of LEL-based detection, total RNA was isolated from THP-1 cells treated with or without NGI-1, an inhibitor of oligosaccharyltransferase, or kifunensine, an inhibitor of α-mannosidase I. Previous studies have shown that both inhibitors suppress glycoRNA biosynthesis (2). Consistent with these findings, treatment with either inhibitor resulted in a marked loss of glycoRNA signal (**Fig. 2b**). We further evaluated specificity by treating total RNA from THP-1 cells with BSA, RNase, DNase I, PNGase F, or proteinase K. As shown in **Fig. 2c**, glycoRNA signals were abolished by RNase and PNGase F treatment, but were unaffected by BSA, DNase I, or proteinase K, indicating that the detected signals depend on both RNA and N-linked glycans. Similarly,

treatment of mouse colon RNA with RNase, but not proteinase K, eliminated the glycoRNA signal (**Fig. 2d**).

Collectively, these results demonstrate that lectin-based detection using LEL exhibits sensitivity and specificity comparable to metabolic labeling and rPAL, and that the detected entities are bona fide glycoRNA molecules. A step-by-step workflow for lectin-based detection of native glycoRNAs is summarized in **Fig. 3.**

Application of LEL to detect native glycoRNAs in physiological and pathological samples

Next, we evaluated whether LEL-based detection could be applied to native glycoRNAs from diverse biological samples. Total RNA was isolated from the cell lines indicated in **Fig. 4a**. GlycoRNAs were highly expressed in human THP-1 cells, differentiated HL-60 (dHL-60) cells, mouse primary neutrophils, and HeLa cells, but were expressed at low levels in HL-60, Jurkat, and HEK293 cells. These expression patterns were consistent with those obtained using rPAL. Because glycoRNAs are localized on the outer surface of cells, we hypothesized that they may be released into the circulation following RNase-mediated cleavage. To test whether free glycoRNAs are present in biofluids, we isolated RNA from human plasma, saliva, urine, feces, and amniotic fluid, as well as from human white blood cells (WBCs), red blood cells (RBCs), and mouse plasma. As shown in **Fig. 4b**, robust glycoRNA expression was detected in human WBCs, consistent with previous reports (11). Notably, strong glycoRNA signals were also detected in human RBCs and plasma. Weaker signals were observed in urine, feces, and amniotic fluid. These findings indicate the presence of free glycoRNAs in human plasma and other biofluids, highlighting their potential utility as biomarkers for disease diagnosis.

We next assessed whether LEL-based detection could be applied to pathological samples. Total RNA isolated from matched normal and cancerous human tissues was obtained from BioChain Institute Inc., with each tissue set derived from a single donor. As shown in **Fig. 4c**, glycoRNA expression was absent or low in normal human breast tissue, detectable in primary breast tumors, and markedly elevated in metastatic breast cancer. Similarly, glycoRNAs were detected in normal human colon tissue, decreased in primary colon cancer, and increased again in metastatic colon cancer relative to the corresponding primary tumors (**Fig. 4c**). These expression patterns suggest that glycoRNAs may play an important role in cancer development and metastasis. Notably, glycoRNAs from metastatic breast cancer tissues exhibited altered electrophoretic mobility compared with those from primary tumors, indicating potential structural differences. Such cancer-associated glycoRNA variants may serve as diagnostic biomarkers or therapeutic targets. Taking together, these results demonstrate that LEL-based detection can be broadly applied to identify native glycoRNAs under both physiological and pathological conditions.

Expression patterns of glycoRNAs across mouse tissues

To profile glycoRNA expression across mouse tissues, we isolated total RNA from 22 tissues obtained from adult C57BL/6 mice. Native glycoRNAs in these tissues were detected using both LEL-based detection and rPAL. As shown in **Fig. 5a**, glycoRNAs were highly expressed in immune-related organs, including thymus, spleen, lymph nodes, bone marrow, and white blood cells (WBCs); gastrointestinal tissues, including esophagus, stomach, intestine, and colon; and several other organs, including brain, heart, white adipose tissue (WAT), and red blood cells (RBCs). In contrast, glycoRNAs were not detectable in cerebellum, lung, liver, kidney, eye, brown adipose tissue (BAT), muscle, or skin. Notably, LEL- and rPAL-based detection yielded highly consistent expression patterns across tissues.

We next compared these results with metabolic labeling. Adult C57BL/6 mice were intraperitoneally injected with Ac_4ManNAz (300 mg/kg/day) for two consecutive days, as described previously (2). Total RNA was then isolated from tissues and analyzed following established protocols (2). Overall, the glycoRNA expression patterns obtained by metabolic labeling were broadly similar, but not entirely consistent, with those detected by LEL and rPAL. For example, glycoRNAs were not detected in brain or bone marrow by metabolic labeling. We speculate that this discrepancy may reflect limited accessibility of the metabolic probe across physiological barriers, such as the blood–brain barrier or blood–bone marrow barrier.

In addition, the electrophoretic migration patterns of glycoRNAs detected by LEL, rPAL, and metabolic labeling were not identical across tissues. rPAL revealed two distinct glycoRNA populations: a slower-migrating species (~11 kb) present in most tissues, and a faster-migrating species (~6 kb) detected primarily in brain, heart, RBCs, WBCs, and colon. These observations suggest the existence of at least two classes of sialylated glycoRNAs with distinct glycan compositions or structural features. Quantification of glycoRNA levels across tissues is shown in **Fig. 5b.**

To further examine glycoRNA expression within the central nervous system, we isolated total RNA from discrete regions of the mouse brain and analyzed glycoRNAs using LEL. GlycoRNAs were highly expressed in the cerebral cortex, midbrain, superior and inferior colliculi, hippocampus, hypothalamus, striatum, and spinal cord, but were undetectable in the cerebellum (**Fig. S2a, b**). We also examined glycoRNA expressions in selected rat tissues and observed expression patterns similar to those seen in mice (**Fig. S3**).

Taken together, these results indicate that while LEL-based detection, rPAL, and metabolic labeling may preferentially detect overlapping but distinct glycoRNA populations, all three approaches provide complementary and valuable tools for investigating glycoRNA biology.

Expression patterns of glycoRNAs across human tissues

To profile glycoRNA expression across human tissues, we obtained 23 commercially available total RNA samples representing distinct tissue types. We first used LEL-based detection to examine glycoRNA expression across these samples. Consistent with observations in mouse tissues, glycoRNAs were highly expressed in WBCs, RBCs, placenta, brain, thymus, and artery. In contrast, glycoRNA expression was not detectable in samples from the gastrointestinal tract, heart, spleen, lymph nodes, bone marrow, or adipose tissue by LEL (**Fig. 6a**), despite their detectability in corresponding mouse tissues.

We next employed rPAL to assess glycoRNA expression in a subset of human tissues. GlycoRNA expression detected by rPAL in human thymus, lung, and placenta was consistent with the results obtained using LEL. Notably, rPAL additionally detected glycoRNA signals in colon, bladder, intestine, stomach, and esophagus, confirming that glycoRNAs are expressed in human gastrointestinal tissues (**Fig. 6b**). The human RNA samples used in this analysis were derived either from single donors or pooled from multiple donors. Due to the high cost and limited availability of these samples, glycoRNA detection was performed only once for each tissue using either LEL or rPAL.

Lectin-detected heterogeneity of glycoRNAs in mouse tissues

According to Vector Laboratories, each lectin binds preferentially to specific sugar moieties with defined linkages. This raises the possibility that different lectins may detect distinct populations of glycoRNAs within cells and tissues. To test this hypothesis, we compared glycoRNA expression patterns in mouse tissues using LEL, WGA, and MAL-II. As shown in **Fig. 7**, LEL and WGA detected similar glycoRNA bands across tissues,

consistent with their shared preference for N-acetylglucosamine. In contrast, MAL-II revealed distinct binding patterns in some tissues. For example, MAL-II detected a glycoRNA band in the cerebellum, whereas LEL and WGA detected none. In the colon, MAL-II detected three bands, whereas LEL and WGA detected one band with long smear. These observations indicate that multiple glycoRNA populations exist in different tissues and that lectins with distinct sugar specificities can be used to reveal the heterogeneity of glycoRNAs in mammalian cells and tissues.

Discussion

Here, we report a relatively simple and rapid lectin-based detection (LBD) method for native glycoRNAs and demonstrate its application in both physiological and pathological samples. We compared LBD with metabolic labeling and rPAL, as summarized in **Fig. 8**. Metabolic labeling relies on incorporation of chemically modified monosaccharides into glycan chains in living cells or animals. After RNA purification and denaturing gel separation, glycoRNAs are detected by labeling modified sialic acids (2). rPAL detects native glycoRNAs in vitro by chemically modifying sialic acid residues after RNA purification (11). In contrast, LBD directly detects glycoRNAs following RNA purification and separation using lectin hybridization. Compared with metabolic labeling and rPAL, LBD offers several advantages: 1) High sensitivity: After optimization, LBD shows comparable sensitivity to metabolic labeling and rPAL. 2) Broader applicability: LBD has broader applications in detecting glycoRNAs from various organisms and the data could provide additional information about other forms of glycoRNAs. 3) Simplified workflow: LBD omits labeling and additional purification steps. 4) Independence from metabolic factors: LBD is not affected by physiological barriers, such as blood–brain or blood–bone marrow barriers.

When comparing expression patterns in mouse tissues, LBD results were largely consistent with rPAL but differed from metabolic labeling. For example, metabolic labeling failed to detect glycoRNAs in the brain and bone marrow, likely due to limited accessibility. Differences in band migration between methods suggest that each technique may detect distinct glycoRNA populations. Using LBD, we also detected free glycoRNAs in human plasma, urine, and amniotic fluid, raising the possibility that circulating glycoRNAs could serve as biomarkers for disease. Preliminary data (Fu, unpublished) indicate that LBD can also detect glycoRNAs in zebrafish, flies, and some bacteria, suggesting that glycoRNAs are evolutionarily conserved and that LBD has broader applicability.

We profiled glycoRNA expressions in human and mouse tissues using LBD, rPAL, and metabolic labeling. GlycoRNAs were highly expressed in immune organs—including thymus, bone marrow, spleen, and lymph nodes—consistent with potential roles in immune cell recruitment, antigen presentation, and signal transduction. High expression was also observed in the gastrointestinal tract (esophagus, stomach, intestine, colon), respiratory system (trachea, lung), bladder, placenta, and uterus, suggesting a potential role for glycoRNAs in membrane barrier function and protection against pathogens. GlycoRNAs were further detected in brain, heart, aorta, white adipose tissue, and RBCs, though their functional significance in these tissues remains to be explored. GlycoRNAs were absent or undetectable in liver, kidney, muscle, skin, eye, cerebellum, brown adipose tissue, and veins but may be expressed in pathological contexts, such as in breast cancer tissues. Notably, glycoRNAs from brain and heart displayed distinct electrophoretic migration patterns, suggesting unique glycan structures in these tissues. Overall, these results indicate that glycoRNAs may play critical roles in immune responses, barrier integrity, host–pathogen interactions, and cancer metastasis.

Interestingly, we observed abundant free glycoRNAs in human plasma and other biofluids, including urine, feces, and amniotic fluids. These glycoRNAs may originate from secreted exosomes or be released from the cell surface of leukocytes, RBCs, or endothelial cells. Because glycoRNAs are stabilized by covalently attached sugar moieties, circulating glycoRNAs could serve as robust biomarkers for disease progression or prognosis. However, current LBD protocols require large plasma volumes, limiting clinical utility. Development of more sensitive, ELISA-based assays for plasma glycoRNA detection is urgently needed.

LBD has some limitations: 1) LBD fails to detect short glycoRNA forms in THP-1 cells, likely due to weak lectin binding; 2) LBD cannot detect glycoRNAs from fixed tissue or directly on the surface of living cells. When we prepared the manuscript, we are happy to see that other groups have developed complementary methods to image cell-surface glycoRNAs (16-20). GlycoRNAs are a newly discovered class of biomolecules. Although many aspects of their biology remain unclear, their importance in both physiological and pathological contexts is emerging (21–32). We anticipate that LBD will serve as a valuable tool for studying glycoRNA biology and may have potential applications in clinical diagnostics.

Materials and Methods

Animals

C57BL/6 mice were purchased from The Jackson Laboratory. At end point, mice were euthanized by administering CO2 in a compressed commercial cylinder with a flow meter rate of 30–70% of the chamber volume/minute for at least 5 min. Cervical dislocation was used as a secondary euthanasia method. All protocols were approved by the University of Missouri–Kansas City (UMKC) Institutional Animal Care and Use Committee (IACUC, protocol# 53601). All experiments were performed in accordance with Public Health Service (PHS) guidelines and regulations and are reported in compliance with the ARRIVE guidelines.

Cell Culture

All cells were maintained at 37 °C in a humidified atmosphere containing 5% CO_2. HeLa and HEK293 cells (ATCC) were cultured in DMEM supplemented with 10% fetal bovine serum (FBS; Thermo Fisher Scientific) and 1% penicillin/streptomycin (P/S, v/v). THP-1, HL-60, and Jurkat cells (ATCC) were cultured in RPMI-1640 medium supplemented with 10% FBS, 1 mM HEPES, 1 mM sodium pyruvate, 0.001% β-mercaptoethanol, and glutamine. Differentiated HL-60 cells (dHL-60) were generated by incubating HL-60 cells with 3% DMSO for 3 days.

Metabolic Labeling of Cells

Stock solutions of N-azidoacetylmannosamine tetraacetate (Ac_4ManNAz; Tocris Bioscience, Cat: 747910) were prepared at 500 mM in sterile dimethyl sulfoxide (DMSO). For cell labeling experiments, Ac_4ManNAz was used at a final concentration of 100 μM. Working stocks of glycan biosynthesis inhibitors were prepared in DMSO and stored at −80 °C: 10 mM NGI-1 (Tocris Bioscience, Cat: 6652) and 10 mM kifunensine (Kif; Tocris Bioscience, Cat: 32071). All compounds were applied to cells for 24 h and were added simultaneously with Ac_4ManNAz.

Metabolic Labeling in Mouse Models

All animal experiments were performed in accordance with guidelines established by the University of South China IACUC committee. C57BL/6 mice were bred in-house. Ac_4ManNAz was prepared by dissolving 100 mg Ac_4ManNAz in 830 μL of 70% DMSO in

phosphate-buffered saline (PBS), warming the solution to 37 °C for 5 min, and sterile filtering through a 0.22 μm centrifugal filter unit (Fisher Scientific). The solution was stored at −20 °C. Male C57BL/6 mice (8–12 weeks old) were injected intraperitoneally once daily with 100 μL Ac_4ManNAz (300 mg/kg/day). Control mice received vehicles alone. After 2 days, mice were euthanized by administering CO_2 in a compressed commercial cylinder with a flow meter rate of 30–70% of the chamber volume/minute for at least 5 min and tissues were harvested. Organs were mechanically dissociated through a nylon cell strainer and resuspended in PBS to generate single-cell suspensions. RNA was extracted as described below.

RNA Extraction and Purification

Total RNA was isolated using TRIzol reagent (Invitrogen, Cat: 15596026) as the initial lysis and denaturation step. Following homogenization by pipetting, samples were incubated at 37 °C for 10 min to disrupt non-covalent interactions. Phase separation was performed by adding 0.2 volumes of chloroform, vertexing thoroughly, and centrifuge at 12,000 × g for 15 min at 4 °C. The aqueous phase was transferred to a new tube and mixed with an equal volume of isopropanol, incubated at 4 °C for 10 min, and centrifuged at 12,000 × g for 10 min at 4 °C. The RNA pellet was washed with 1 mL of 75% ethanol, air-dried at room temperature, and resuspended in RNase-free water.

Following enzymatic treatment or biotin conjugation, RNA samples were purified using Zymo RNA purification columns (Zymo Research, Cat: R1017) according to the manufacturer's instructions. Human blood, saliva, urine, fecal matter, amniotic fluid samples were purchased from Innovative Research and Amsbio as deidentified samples. For plasma, saliva and amniotic fluid RNA isolation, 250 μL of sample was mixed with 750 μL TRIzol-LS (Invitrogen, Cat: 10296010). For urine samples, urine was concentrated tenfold using Amicon centrifugal filters before TRIzol-LS extraction. For fecal samples, 1 g of feces was mixed with PBS by rotation for 1 h, centrifuged at 12,000 × g for 10 min at 4 °C, and the supernatant was extracted using TRIzol-LS. Subsequent steps were performed as described above.

Enzymatic Treatment of RNA

For enzymatic digestion, 1 μL of RNase cocktail (0.5 U/μL RNase A and 20 U/μL RNase T1; Thermo Fisher Scientific), DNase I (Zymo Research), Proteinase K (Thermo Fisher Scientific), or PNGase F (New England Biolabs) was added to 20 μL of total RNA and incubated at 37 °C for 10 min. Reactions were purified using Zymo RNA purification columns.

Copper-Free Click Conjugation to RNA

All click chemistry reactions were performed under copper-free conditions to avoid copper-induced RNA damage. Dibenzocyclooctyne-PEG4-biotin (DBCO-biotin; Tocris Bioscience, Cat: 7480) was used for strain-promoted azide–alkyne cycloaddition (SPAAC). RNA in nuclease-free water was mixed with an equal volume of dye-free gel loading buffer II (df-GLBII; 95% formamide, 18 mM EDTA, 0.025% SDS) and 500 μM DBCO-biotin. Typical reaction volumes consisted of 30 μL df-GLBII, 27 μL RNA, and 3 μL of 10 mM DBCO-biotin stock. Reactions were incubated at 55 °C for 10 min and terminated by addition of RNA binding buffer followed by ethanol precipitation. RNA was purified using Zymo columns.

RNA Gel Electrophoresis, Blotting, and Imaging

Blotting analysis of Ac_4ManNAz-labeled RNA was performed as described by Flynn et al., with modifications. RNA was eluted from columns in 18 μL water, mixed with 18 μL df-GLBII containing ethidium bromide, heated at 55 °C for 10 min, and chilled on ice.

Samples were resolved on 1% agarose-formaldehyde denaturing gels (NorthernMax kit, Invitrogen, AM1940) at 60 V for 60 min. Total RNA was visualized using an iBright 1500 imaging system. RNA was transferred to 0.45 µm nitrocellulose membranes following the NorthernMax protocol and UV-crosslinked (0.18 J/cm^2). Membranes were blocked with protein-free blocking buffer (LI-COR Biosciences, Cat: 927-90001) for 1 h at room temperature and incubated with anti-biotin-HRP (1:1000; Thermo Fisher Scientific, PA1-30595) at 4 °C for 2–16 h. Membranes were washed with 0.1% Tween-20 in PBS and imaged using the iBright 1500.

rPAL

RNA periodate-alkyne ligation (rPAL) was performed as described by Xie et al. Briefly, RNA (3–10 µg) was incubated with blocking buffer containing mPEG3-aldehyde, $MgSO_4$, and NH_4OAc (pH 5) at 35 °C for 45 min. Aldehyde-reactive probe (ARP) was added followed by sodium periodate oxidation for exactly 10 min at room temperature in the dark. Oxidation was quenched with sodium sulfite, and ligation was allowed to proceed at 35 °C for 90 min. RNA was purified using Zymo columns and eluted in nuclease-free water.

LBD

The step-by-step protocol for LBD is summarized in **Figure 3**. A patent application for this method is pending.

Reagents

Lectins (including LEL, Vector Lab, L-1170-2) and Ac_4ManNAz were purchased from Vector Laboratories. Human tissue RNAs were obtained from Biochain Institute Inc., and human thymus RNA was from AMSBIO. The NorthernMax kit was purchased from Invitrogen, protein-free blocking buffer from LI-COR Biosciences, mPEG3-aldehyde from Creative Labs, and anti-biotin-HRP antibodies and nitrocellulose membranes from Thermo Fisher Scientific. All cell lines were obtained from ATCC and provided by collaborators.

Acknowledgments

We thank Drs. Tony Wang, Daping Fan, Kun Chen, Jianming Qiu, Shizhen Wang, and Cuthbert Simpkins for kindly providing cell lines and/or RNA samples.

Author Contributions

M.F. conceived, designed, and supervised the overall study. Y.L., X.L., and M.F. performed most of the experiments. Y.Q. performed the metabolic labeling experiments in mice. T.L. and P.N. assisted with mouse tissue expression experiments. M.F. wrote the manuscript. M.F., H.M., and P.N. revised and edited the manuscript. All authors approved the final version of the manuscript.

Funding

This work was supported by the National Institutes of Health (R15AI138116 to M.F.), UMKC Funding for Excellence (2023 to M.F.), SPiRE (2024 to M.F.), and the UMKC School of Medicine Bridge Fund (2025 to M.F.).

Declaration of Competing Interests

The authors declare no competing interests.

Data Availability

The datasets generated and/or analyzed during the current study are available from the corresponding author upon reasonable request.

References

1. Huang, N. *et al.* Natural display of nuclear-encoded RNA on the cell surface and its impact on cell interaction. Genome Biol. *21*, 225 (2020).
2. Flynn, R. A. *et al.* Small RNAs are modified with N-glycans and displayed on the surface of living cells. Cell *184*, 3109–3124.e22 (2021).
3. Li, Z. *et al.* Cell-surface RNA forms ternary complex with RNA-binding proteins and heparan sulfate to recruit immune receptors. Mol. Cell *85*, 4633–4650.e11 (2025).
4. Zhang, N. *et al.* Cell surface RNAs control neutrophil recruitment. Cell *187*, 846–860 (2024).
5. Li, Y. *et al.* GlycoRNA-L and glycoRNA-S mediate human monocyte adhesion via binding to Siglec-5. Biochim. Biophys. Acta Mol. Cell Res. *1872*, 120017 (2025).
6. Graziano, V. R. *et al.* RNA N-glycosylation enables immune evasion and homeostatic efferocytosis. Nature *645*, 784–792 (2025).
7. Jiang, X. *et al.* Deciphering the RNA landscapes on mammalian cell surfaces. Protein Cell, 13: pwaf079 (2025).
8. Abledu, J. K. *et al.* Cell surface RNA expression modulates alveolar epithelial function. Am. J. Respir. Cell Mol. Biol. *73*, 466–478 (2025).
9. He, J. *et al.* The role of cell surface RNAs in hepatocellular carcinoma. Int. J. Biol. Macromol. *330*, 147948 (2025).
10. Xin, B. *et al.* GlycoRNAs are abundant in glioma and involved in glioma cell proliferation. Oncogenesis *14*, 29 (2025).
11. Xie, Y. *et al.* The modified RNA base acp3U is an attachment site for N-glycans in glycoRNA. Cell (2024).
12. Perr, J. *et al.* RNA-binding proteins and glycoRNAs form domains on the cell surface for cell-penetrating peptide entry. Cell *188*, 1878–1895.e25 (2025).
13. Li, L. *et al.* Protocol for detecting glycoRNAs using metabolic labeling and northwestern blot. STAR Protoc. *5*, 103321 (2024).
14. Awofiranye, A. E. *et al.* N-glycolylated carbohydrates in nature. Glycobiology *32*, 921–932 (2022).
15. Sharma, S. *et al.* Extracellular exosomal RNAs are glyco-modified. Nat. Cell Biol. *27*, 983–991 (2025).
16. Ma, Y. *et al.* Spatial imaging of glycoRNA in single cells with ARPLA. Nat. Biotechnol. *42*, 608–616 (2024).
17. Ren, T. *et al.* FRET imaging of glycoRNA on small extracellular vesicles enabling sensitive cancer diagnostics. Nat. Commun. *16*, 3391 (2025).
18. Gong, Z. *et al.* Intramolecular proximity-induced amplification for accurate imaging of glycosylated RNAs in living cells and zebrafish. Anal. Chem. *97*, 20897–20907 (2025).
19. Brunner, C. M. *et al.* Bottom-up investigation of spatiotemporal glycocalyx dynamics with interferometric scattering microscopy. J. Am. Chem. Soc. *147*, 32799–32808 (2025).
20. Ge, J. *et al.* Comprehensive and facile strategy for enhanced visualization of sialylated RNA via dual bioorthogonal labeling. ACS Chem. Biol. *20*, 1884–1891 (2025).
21. Hazemi, M. E. *et al.* An expanded view of RNA modification with carbohydrate-based metabolic probes. JACS Au *5*, 2309–2320 (2025).

22. Muller, W. A. A physiological role for cell surface glycoRNAs. J. Leukoc. Biol. *115*, 996–998 (2024).
23. Chokkalla, A. K. *et al.* Immunomodulatory role of glycoRNAs in the brain. J. Cereb. Blood Flow Metab. *43*, 499–504 (2023).
24. Nachtergaele, S. & Krishnan, Y. New vistas for cell-surface glycoRNAs. N. Engl. J. Med. *385*, 658–660 (2021).
25. Chai, P., Lebedenko, C. G. & Flynn, R. A. RNA crossing membranes: systems and mechanisms contextualizing extracellular RNA and cell surface glycoRNAs. Annu. Rev. Genomics Hum. Genet. *24*, 85–107 (2023).
26. Chevet, E., De Matteis, M. A., Eskelinen, E.-L. & Farhan, H. RNA, a new member in the glycan club that gets exposed at the cell surface. Traffic *22*, 362–363 (2021).
27. Porat, J. & Flynn, R. A. Cell surface RNA biology: new roles for RNA-binding proteins. Trends Biochem. Sci. (2025).
28. Li, H. *et al.* GlycoRNAs: more than the intersection of glycobiology and RNA biology. Life Med. *3*, lnae044 (2024).
29. Chen, X. *et al.* Potential function of glycosylated RNA in diseases. Wiley Interdiscip. Rev. RNA *16*, e70031 (2025).
30. Li, B. *et al.* GlycoRNAs as emerging drug targets. Trends Pharmacol. Sci. *46*, 832–835 (2025).
31. Montag, N. *et al.* The emerging role of glycoRNAs in immune regulation and recognition. Immunol. Lett. *276*, 107048 (2025).
32. Kim, H. S. GlycoRNA: a new player in cellular communication. Oncol. Res. *33*, 995–1000 (2025).

Figure Legends

Figure 1. Screening of lectins for detection of native glycoRNAs.
(a) Twenty-four lectins were purchased from Vector Laboratories and screened for their ability to detect native glycoRNAs. Total RNA (10 µg) isolated from THP-1 cells was used for lectin screening. As a positive control, input RNA (10 µg) isolated from Ac_4ManNAz-labeled THP-1 cells was conjugated with biotin and detected using anti-biotin-HRP. All lectins were used at a concentration of 1.5 µg/mL. Experiments were repeated twice.
(b) Band intensities were quantified using iBright internal software. Information on the primary sugar specificity of lectins was obtained from Vector Laboratories.

Figure 2. Sensitivity and specificity of lectin-based detection of native glycoRNAs.
(a) Sensitivity comparison of the three indicated detection methods. Increasing amounts of total RNA isolated from Ac_4ManNAz-labeled or unlabeled THP-1 cells were analyzed.
(b) Total RNA (10 µg) from THP-1 cells treated with or without NGI-1 (4 µM) or kifunensine (Kif; 1 µM) was analyzed by lectin-based detection (LBD) using LEL (3 µg/mL).
(c) Total RNA (10 µg) from THP-1 cells was treated with RNase cocktail (1 µL; RNase A, 0.5 U/µL and RNase T1, 20 U/µL), DNase I (1 U/µL), PNGase F (1 U/µL), or Proteinase K (2 µg/µL) at 37 °C for 10 min. After purification using Zymo columns, samples were analyzed by LBD with LEL (3 µg/mL).
(d) Total RNA (10 µg) from mouse colon tissue was treated with RNase cocktail, DNase I (1 U/µL), or Proteinase K (2 µg/µL) at 37 °C for 10 min. After purification, RNA samples were analyzed by LBD using LEL (3 µg/mL). All experiments were repeated twice.

Figure 3. Step-by-step protocol for lectin-based detection of native glycoRNAs.

Figure 4. Detection of native glycoRNAs in physiological and pathological samples.
(a) Native glycoRNAs in the indicated cell lines were detected using LEL (3 μg/mL) and rPAL. Total RNA (10 μg) was analyzed. Experiments were repeated twice, and band intensities were quantified using iBright internal software.
(b) RNA (2–5 μg) isolated from human blood cells, plasma, saliva, urine, feces, amniotic fluid, and mouse plasma was analyzed by LEL-based detection (3 μg/mL).
(c) Total RNA isolated from human normal breast or colon tissues (N), primary tumors (P), or metastatic tumors (M) were analyzed using LEL (3 μg/mL).

Figure 5. Expression patterns of glycoRNAs in mouse tissues.
(a) GlycoRNA expression in mouse tissues was analyzed using three methods: LBD (LEL, 3 μg/mL), rPAL, and metabolic labeling, as indicated. Total RNA (10–15 μg) was analyzed. Experiments were biologically repeated at least twice.
(b) Quantification of glycoRNA levels in mouse tissues was performed using iBright software.

Figure 6. Expression patterns of glycoRNAs in human tissues.
GlycoRNA expression in human tissues was analyzed by LBD using LEL (3 μg/mL) (a) and by rPAL (b), as indicated. Total RNA (8–10 μg) was used for analysis.

Figure 7. Lectin-detected heterogeneity of glycoRNAs in mouse tissues.
GlycoRNA expression in different mouse tissues was analyzed using LEL, WGA, or MAL-II (each at 3 μg/mL). Total RNA (10–15 μg) was analyzed.

Figure 8. Schematic comparison of metabolic labeling, rPAL, and LBD procedures.

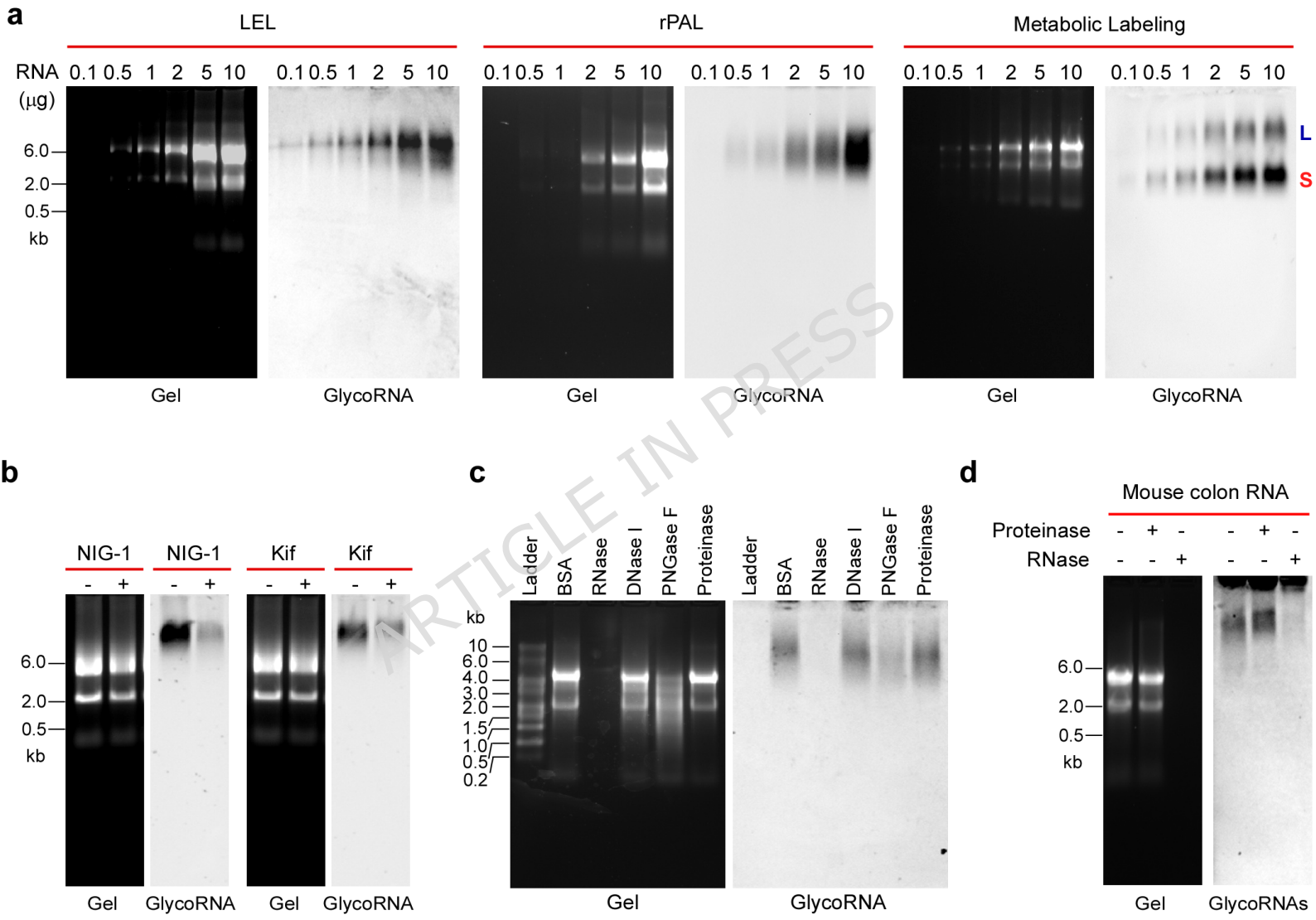

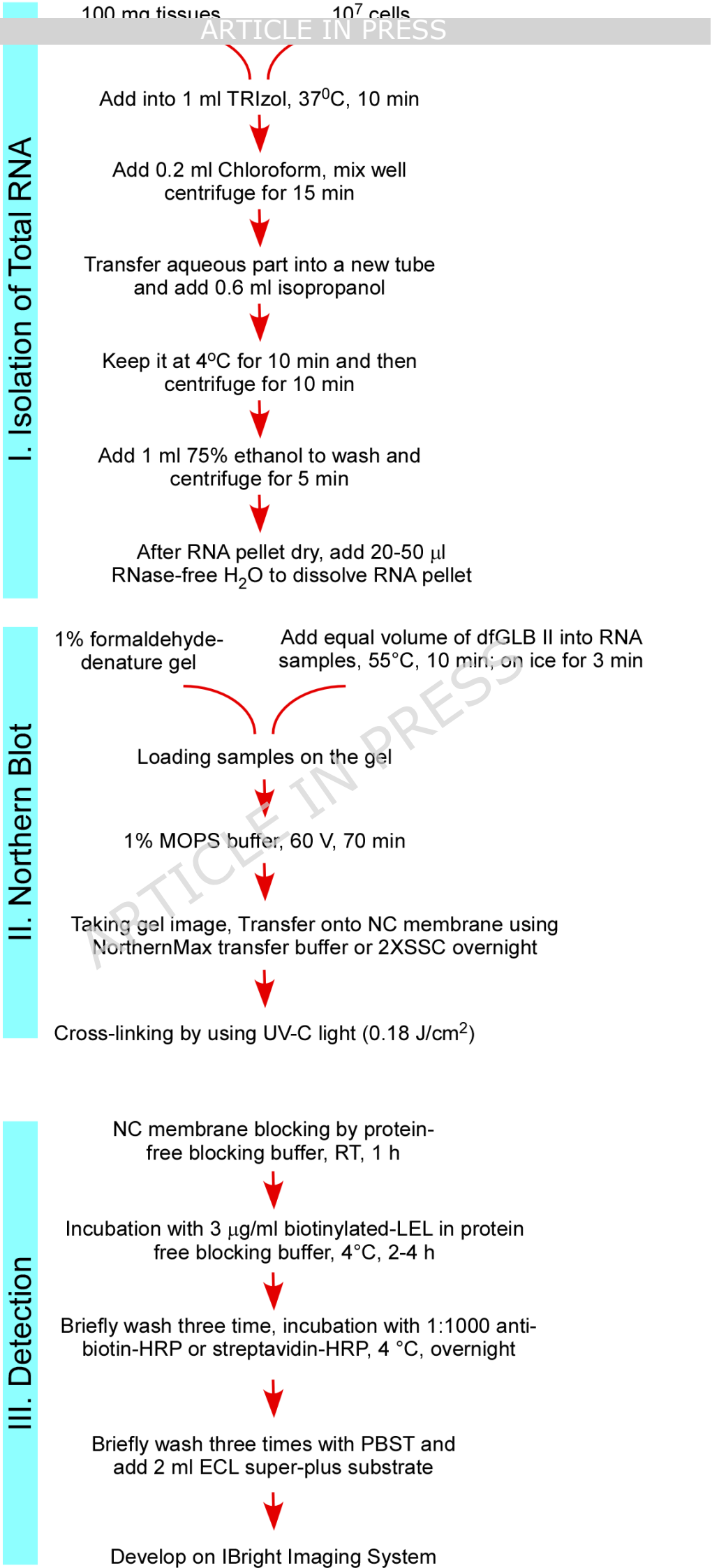

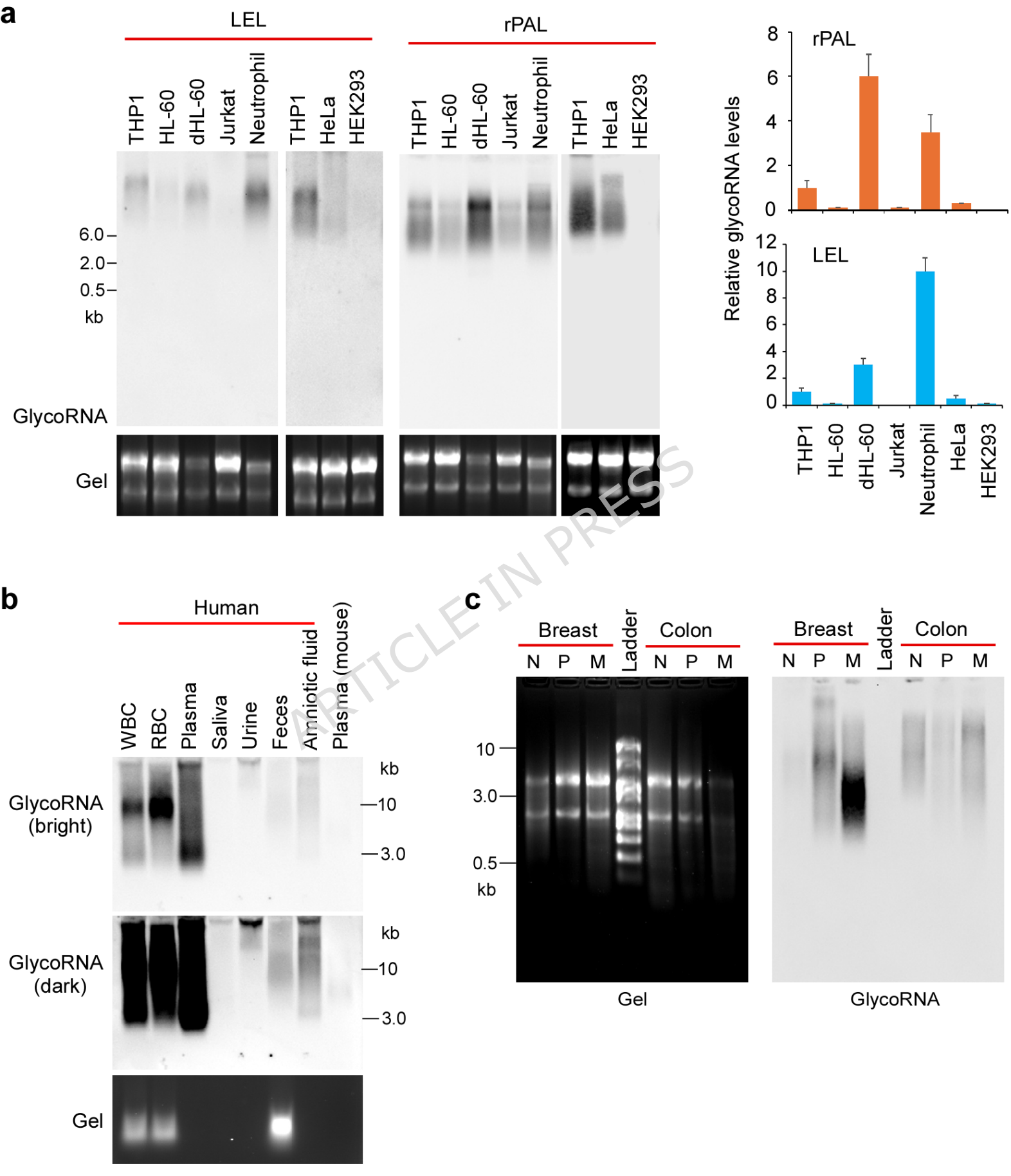

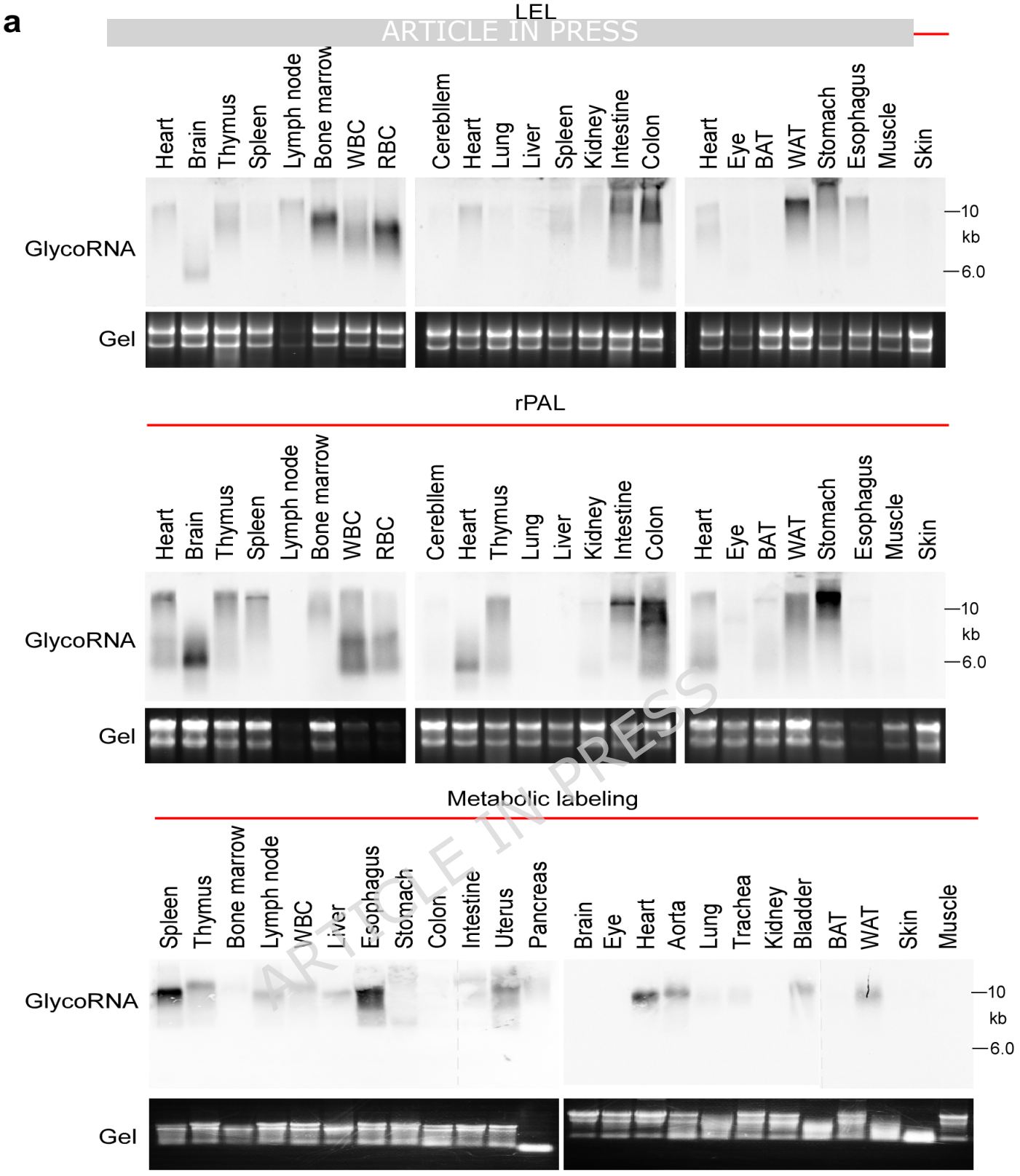

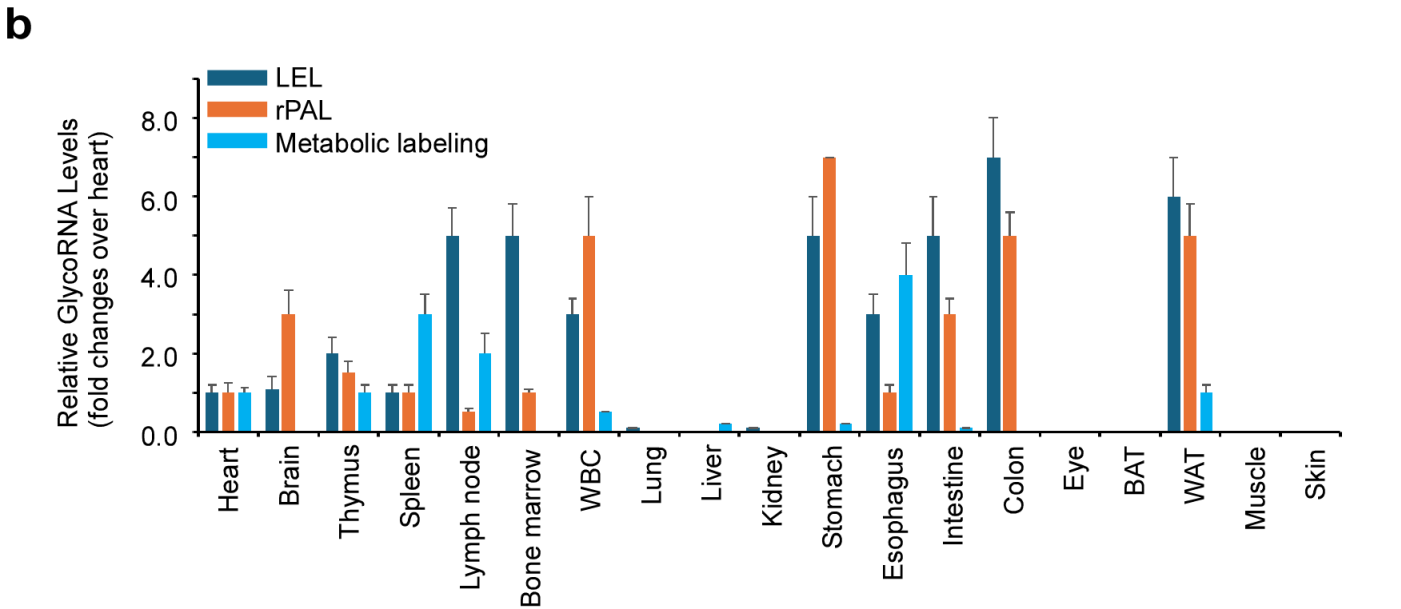

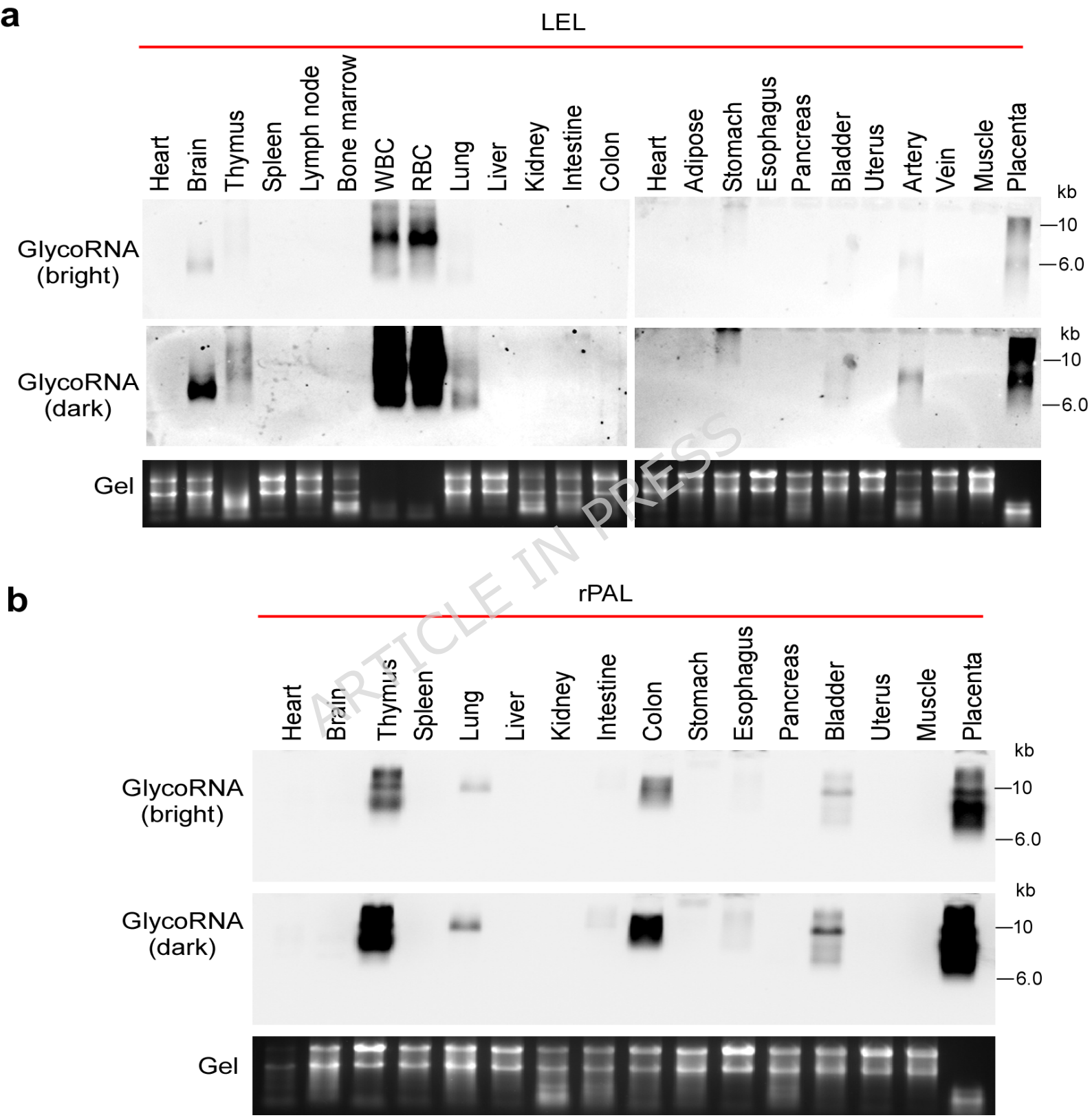

LEL

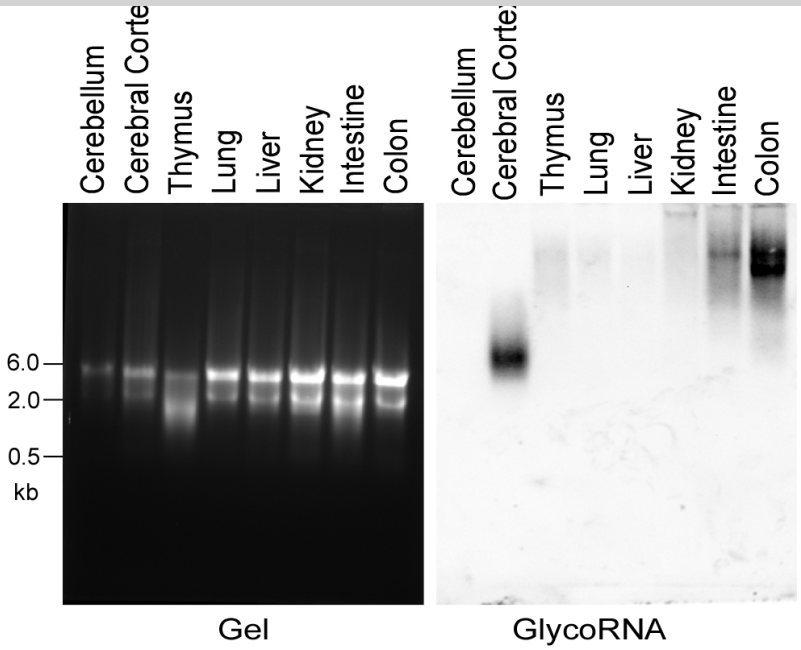

WGA

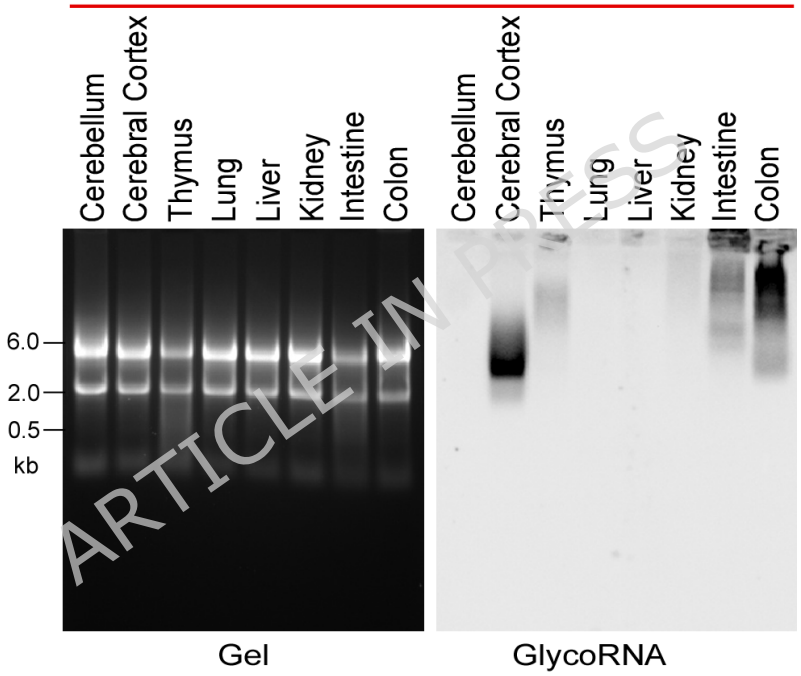

MAL-II

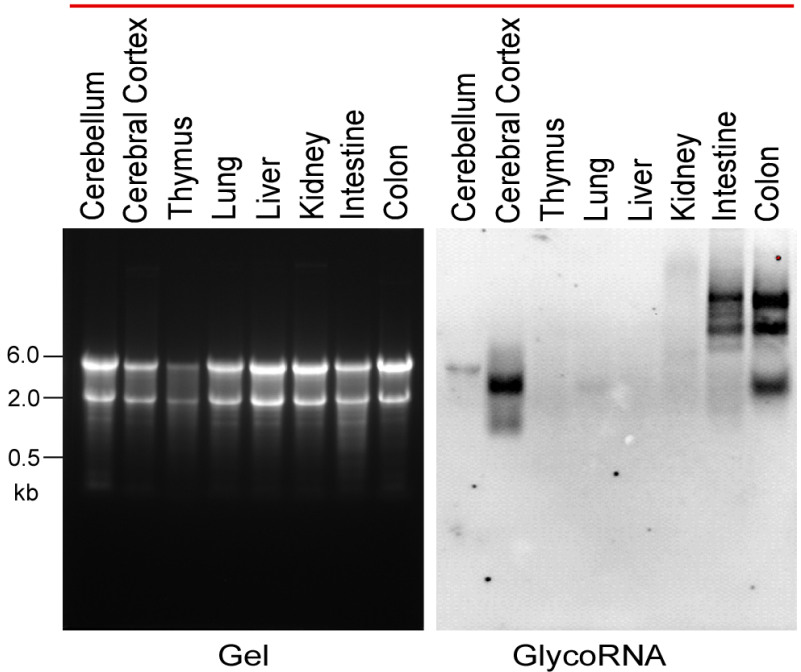

Metabolic Labeling

1. Labeling

2. RNA purification

3. Biotin conjugation

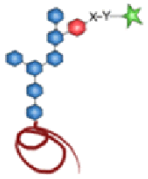

4. Reaction purification

5. Northern blotting

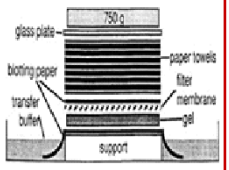

6. Detection

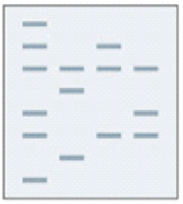

rPAL

1. RNA purification

2. Diol oxidation + aldehyde ligation

3. Reaction purification

4. Northern blotting

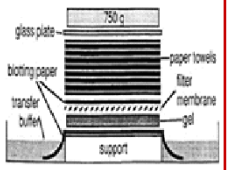

5. Detection

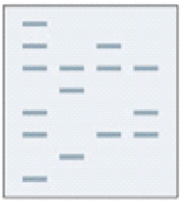

LBD

1. RNA purification

2. Northern blotting

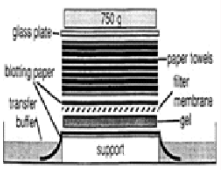

3. LEL hybridization

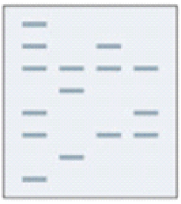

4. Detection

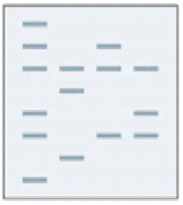

a

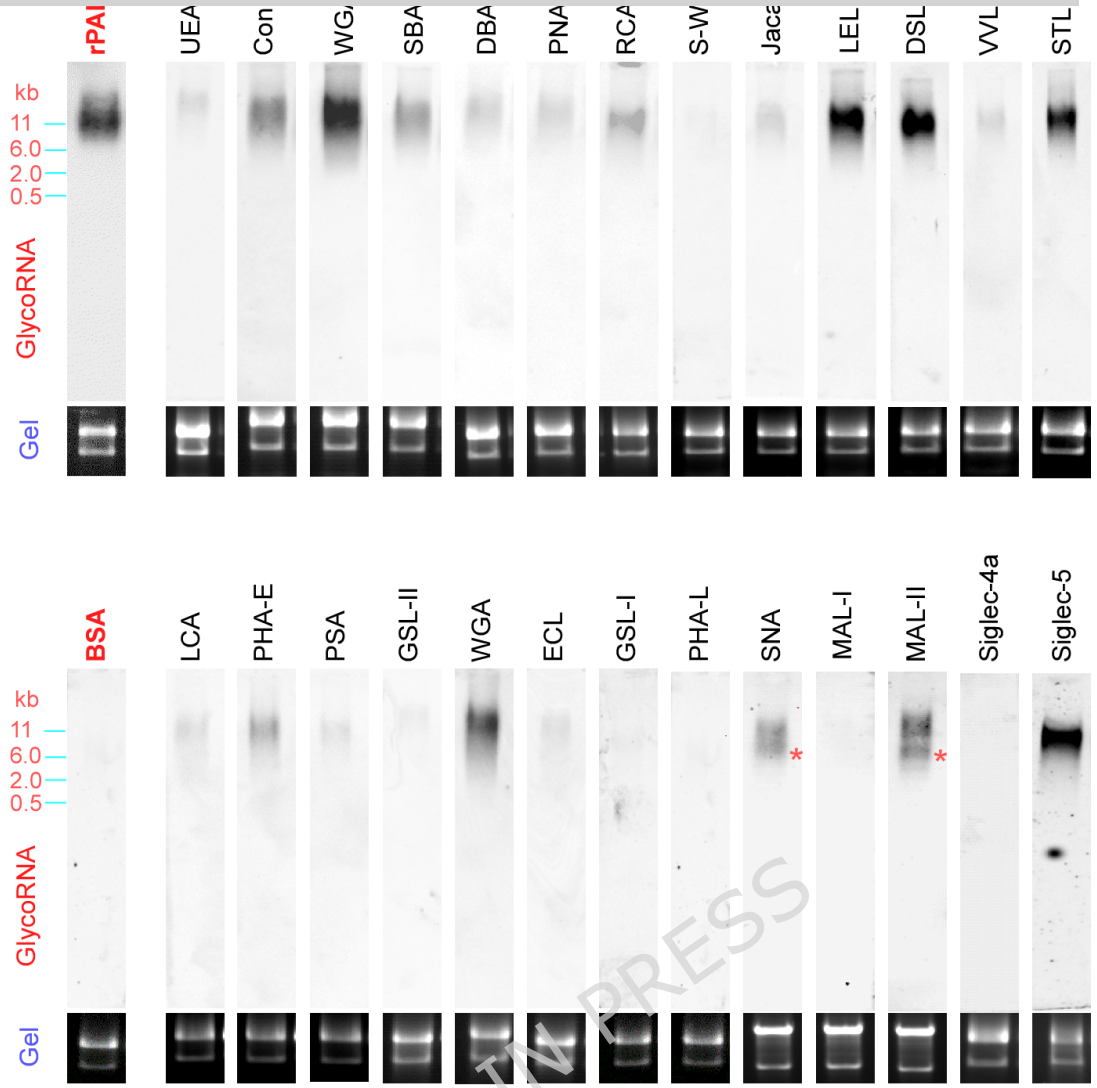

b